ACS Energy LETTERS

http://pubs.acs.org/journal/aelccp

Mitigating the High-Charge Detrimental Phase Transformation in $LiNiO_2$ Using Doping Engineering

Jianli Cheng, Bin Ouyang, and Kristin A. Persson*

Cite This: *ACS Energy Lett.* 2023, 8, 2401−2407

Read Online

ACCESS | Metrics & More | Article Recommendations | Supporting Information

ABSTRACT: Cobalt-free layered $LiNiO_2$ has gained increased interest due to the scarcity and high cost of cobalt. However, $LiNiO_2$ suffers from poor cycling stability, which is mainly due to oxygen loss and structural instability, especially when operating at high voltages. Herein, we present a doping strategy to mitigate the detrimental O3-to-O1 phase transformation in $LiNiO_2$ from first-principles calculations. Temperature−composition phase diagrams of pristine and doped $Li_{1-x}NiO_2$ are obtained using a cluster-expansion and Monte Carlo simulation approach. We investigate the effects of dopant oxidation states, sizes, and concentrations on the dopant distribution in $LiNi_{1-y}M_yO_2$ (M = Sb, Ti, Si, Al, and Mg) as well as the phase transitions during delithiation. We find that introducing high-valence dopants with ionic radii similar to that of Ni^{3+} into $LiNiO_2$ stabilizes the O3-phase cathode bulk structure at high charge. Our results provide a general guidance on using doping engineering to realize Ni-rich, Co-free cathodes for lithium-ion batteries.

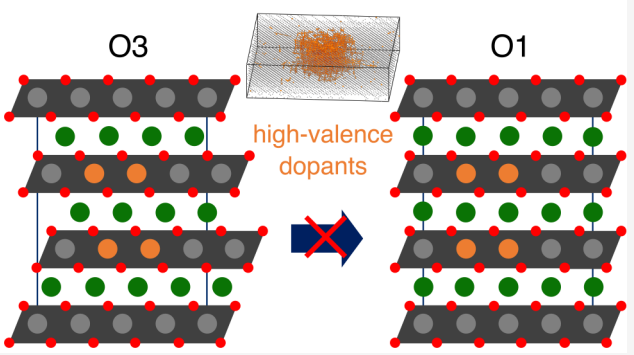

In the past decade, lithium-ion batteries (LIBs) have become the dominant power source for electric vehicles (EVs) and plug-in hybrid EVs (PHEVs) due to the dramatically reduced cost of an LIB pack from approximately US$1,200/kWh to approximately US$150/kWh in 2022.[1] However, the projected increase of the EV market[1,2] necessitates a re-evaluation of the metals used in the cathodes of LIBs, especially cobalt, which is not mined at the scale needed to sustain such growth. Indeed, the current cathode family of choice for the EV market, the layered oxide cathodes, i.e., $Li[Ni_{1-y-z}Co_yAl_z]O_2$ (NCA) and $Li[Ni_{1-y-z}Co_yMn_z]O_2$ (NCM), has undergone a steep increase in the Ni content and a corresponding decrease in the Co content from, e.g., NCM111 (33% Ni, 33% Co) to today's NCM622 (60% Ni, 20% Co) and NCM811 (80% Ni, 10% Co) compositions.[3]

The ultimate end member of the NCA and NCM families is $LiNiO_2$, which exhibits the highest theoretical capacity (275 mAh/g). However, the challenges that accompany its high specific capacity are substantially compromised cycling and thermal stability.[4,5] During cycling, $LiNiO_2$ undergoes a series of phase transitions, whereof one, comprising of a shift from O3 to O1 oxygen stacking (sometimes denominated H2 to H3) at high potentials (V > 4.1 V), leads to extensive structural damages of the cathode particles and a rapid capacity fade.[4] Figure 1 illustrates the change in oxygen stacking and the corresponding O3, O1, and O1-3 phases in $LiNiO_2$. Specifically, at low Li content (less than 25% Li left),[6,7] a two-phase region of O3+O1 emerges with heterogeneous Li

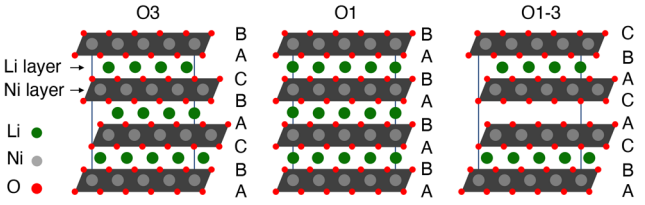

Figure 1. Schematic illustration of three host structures O3, O1, and O1-3. In the O3 oxygen stacking, the Li octahedrons share edges with the surrounding Ni octahedrons, while they share faces in the O1 oxygen stacking. The O1-3 host has alternating O3 and O1 oxygen stacking, and Li ions only occupy the layers with an O3 oxygen stacking.

Received: January 23, 2023
Accepted: April 11, 2023

https://doi.org/10.1021/acsenergylett.3c00169
ACS Energy Lett. 2023, 8, 2401−2407

distribution as the O1 phase is devoid of Li. Because of the Li depletion, the lattice contracts anisotropically and abruptly.[6,7] Such lattice contraction is worsened by the presence of the O1 phase.[8] Simultaneously, the formation of the O1 phase creates stacking faults in the layered structure because of the different oxygen stacking sequences (see Figure 1). Both these factors contribute to a strain-induced structural instability of the cathode, which typically manifests in the formation of microcracks.[8] Recent studies also showed that the O1 phase could act as a nucleation site to (1) initialize cracking from the cathode particle surface and (2) provide diffusion pathways for oxygen loss, thereby promoting the irreversible transformation from the layered structure into a densified rocksalt structure.[9,10] Therefore, to develop the next-generation Ni-rich layered cathodes, it is critical to suppress the O1 phase formation. While the structural instability can be avoided by simply limiting the upper cutoff voltage to 4.1 V, this remedy comes at the cost of a decreased specific capacity.[4] Hence, it has been deemed a priority to develop Ni-rich, Co-free cathodes for next-generation EV batteries where the trade-off between specific capacity and cycling stability is mitigated.[11]

One such proposed strategy is to introduce doping elements to develop non-standard cathode chemistries.[3,11,12] In this context, $LiNiO_2$ provides a fertile chemical playground for compositional design of Ni-rich, Co-free cathode alternatives to the standard NCA and NCM chemistries. A range of dopants have been proposed to mitigate the O3-to-O1 phase transition and promote a more stable $LiNiO_2$ structure at high charge. Such dopants include W,[13] Nb,[14] Ti,[15] Mn,[16] Ga,[17] Al,[18] Cu,[19] and Mg.[15] In addition, some of these dopants have been proposed to exhibit a stabilizing effect on other high-energy-density layered cathodes. For example, Levartovsky et al. reported that 1% W doping effectively suppresses the O3-to-O1 phase transition in $LiNi_{0.85}Co_{0.1}Mn_{0.05}O_2$.[20] Similarly, Nayak et al. reported that 5% Al doping mitigates the layered-to-spinel phase transition and thereby improves the cycling performance of Li- and Mn-rich cathodes.[21] Despite the enthusiasm for doping engineering in the design of Co-free cathodes, there is still a lack of understanding about the dopant role for $LiNiO_2$ or Ni-rich cathodes in general. In addition, since both dopant chemistry and concentration influence a variety of short-range as well as long-range materials properties, it is experimentally challenging to interpret and deconvolute their effects on the cycling and capacity retention. For example, Guilmard et al. reported that 10% Al doping in $LiNi_{1-y}Al_yO_2$ is sufficient to suppress the phase transition and improve the cycling stability.[22] Cao reported that 5% Al is the optimal doping concentration to achieve a uniform doping distribution and the best cycling performance compared to other Al doping concentrations and pristine $LiNiO_2$,[18] while Park et al. reported that 1% Al doping does not lead to a noticeable cycling performance improvement in $LiNi_{0.9}Mn_{0.1}O_2$.[12] On the other hand, modeling is a powerful tool to help identify the intrinsic impact of composition and doping engineering on electrochemical performance, avoiding effects of synthesis and cell processing. Indeed, numerous theoretical studies on doping engineering of $LiNiO_2$ have also been reported.[3,23−25] For example, Yoshida et al. performed an *ab initio* screening of dopant effects on lattice contraction in $Li(Ni_{0.75}Co_{0.17}X_{0.08})O_2$ by calculating the layer spacing change in the O3 phase. In this work, Ni was substituted by various dopants and Nb was identified as a promising agent to minimize lattice contraction during cycling.[26] Similarly, Kong et al. studied anion doping effects on the structural stability of $LiNiO_2$ by calculating lattice contractions and Ni migration in the O3 phase. They found Cl to be a promising dopant to reduce lattice contraction and that F may mitigate Ni migration.[27] Recently, Mock et al. used lattice models to calculate the voltage profiles of pristine and Al-doped $LiNiO_2$ in the O3 phase. They reported that the two-phase plateau at low Li content (less than 25% Li left) in $LiNiO_2$ can be effectively suppressed with 10% Al-doping, which indicates a structural stabilization.[28] However, to our best knowledge, there has been no systematic theoretical investigation of the doping effects on the phase evolution of $LiNiO_2$, considering both O3 and O1 phases, as a function of dopant concentration. Indeed, experimental evidence shows that dopant concentration in Ni-rich cathodes can significantly impact batteries' cycling performance[12,22,29,30] and that dopant distribution behavior is specific to the chemistry of the dopant.[3,15]

In this study, we implement a first-principles, cluster-expansion and Monte Carlo approach to study $LiNiO_2$ doped with a series of dopant elements with varying valence states (Sb^{5+}, Ti^{4+}, Si^{4+}, Al^{3+}, and Mg^{2+}) to 1) obtain clarification on the direct role of the dopants as suppressants of the O1 phase at high charge and 2) provide general guidelines of dopant selection to improve the structural stability of Ni-rich and Co-free cathodes. We investigate the effects of dopant oxidation state, size, and concentration on dopant distribution in $LiNi_{1-y}M_yO_2$ (M = Sb, Ti, Si, Al, and Mg). We compare the phase stability of the O3, O1, and O1-3 phases as a function of Li concentration and temperature and calculate the phase diagrams of pristine and doped $LiNiO_2$. The inclusion of the O1-3 phase corresponds to recent experimental reports of discrete O3 and O1 domains in charged Ni-rich cathodes.[9,10] Combining our results with previously reported experimental studies, we recommend to introduce high-valence dopants with ionic radii similar to that of Ni^{3+} into Ni-rich and Co-free cathodes. This approach could potentially stabilize both surface and bulk structures of the cathode material.

Pristine $LiNiO_2$. To clearly illustrate the effects of dopants, we first reproduce the known phase behavior in pristine $LiNiO_2$ as a baseline. In Figure 2a, we plot the calculated composition−temperature phase diagram of $Li_{1-x}NiO_2$, which contains four single-phase regions separated by domains of two-phase regions. Thus, all phase transitions are first order, with a variety of intermediate ordered phases at x = 0.25, 0.5, and 0.75. For less than 75% delithiation (x < 0.75) all $Li_{1-x}NiO_2$ structures exhibit the O3 phase, which has been found to correlate with a stable bulk structure and cycling performance.[4] Each two-phase region at x < 0.75 (hatched areas) is formed between two O3 structures with different Li ordering and concentration. Upon further delithiation (x > 0.75), a two-phase region comprising the O3 and O1-3 phases emerges. The O1-3 phase exhibits O1 oxygen stacking which has been reported to promote cracking and oxygen loss.[9,10] Therefore, the formation of O1 oxygen stacking indicates an emergent structural instability at x > 0.75, likely contributing to structural damage and deteriorated cycling stability.[4] This is in excellent agreement with experimental observations, which reported that the maximum rechargeable capacity is 200 mAh/g with x = 0.75 in $Li_{1-x}NiO_2$.[6] A two-phase region with large lattice contraction appears for x > 0.75.[6] Yoon et al. reported detrimental phase transition and extensive structural damages after cycling $LiNiO_2$ particles above 4.2 V (x > 0.8).[4] Notably,

https://doi.org/10.1021/acsenergylett.3c00169
ACS Energy Lett. 2023, 8, 2401−2407

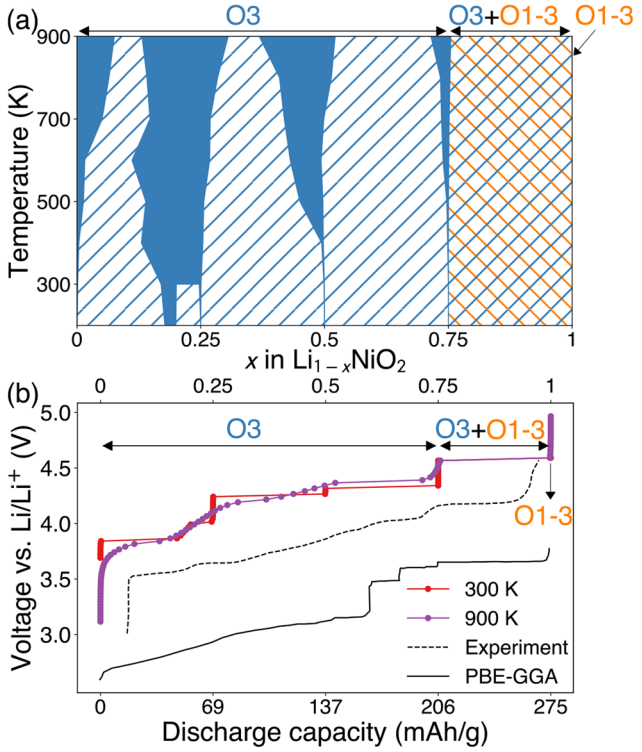

Figure 2. (a) Calculated $Li_{1-x}NiO_2$ phase diagram as a function of temperature and Li concentration. The blue solid areas represent solid solution regions of $Li_{1-x}NiO_2$ and the hatched areas represent two-phase regions. Blue and orange represent O3 and O1-3 phase, respectively. (b) Comparison between calculated and experimental voltage profiles of $LiNiO_2$. The experimental data is from ref 7. We also show a calculated voltage curve from ref 31.

Figure 2a shows that the destructive O3+O1-3 two-phase region remains at high temperatures. Our calculated voltage profile of $Li_{1-x}NiO_2$ also agrees with the experimental one. Figure 2b illustrates the calculated voltage profiles of pristine $LiNiO_2$ at 300 and 900 K as a function of discharge capacity and composition. Each plateau corresponds to a two-phase region, whereas the single-phase regions are characterized by continuous changes in the cell voltage, which are reflected in the calculated phase diagram. For comparison, we also plot previously measured experimental and calculated voltage profiles of $LiNiO_2$ from Li et al.[7] and Arroyo y de Dompablo et al.,[31] respectively, in Figure 2b. Our calculated voltage overpredicts the experimental value by about 0.4 V, whereas Arroyo y de Dompablo et al. underpredicted the value by about 0.5 V, a difference that is attributed to the *U* value for the Ni 3*d* orbitals (the generalized gradient approximation (GGA) was used in ref 31). Nevertheless, our voltage profile correctly reflects the intercalation reaction mechanism during the charging of $LiNiO_2$, and the shape of the voltage curve qualitatively agrees with the experimental results, especially the voltage plateau at $x > 0.75$. Some minor variances are noted between the computed and experimental results for the phase behavior between $0 < x < 0.75$. For example, we identify a two-phase region at $0.5 < x < 0.75$, whereas it is reported at $0.6 < x < 0.7$ in Li et al.'s study.[7]

Doped $Li_{1-x}Ni_{1-y}M_yO_2$, *M* = Sb, Ti, Si, Al, and Mg. For each dopant case, we investigate the dopant spatial distribution in $LiNi_{1-y}M_yO_2$. Figure 3 illustrates the dopant distribution behaviors for Sb, Ti, Si, Al, and Mg in O3 $LiNi_{0.95}M_{0.05}O_2$ host

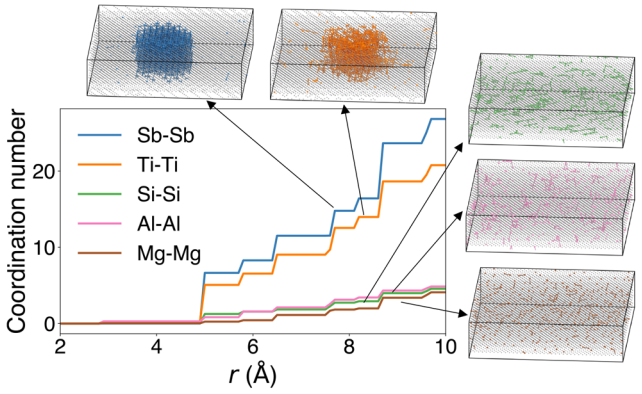

Figure 3. Dopant−dopant coordination numbers as a function of dopant−dopant distance in $LiNi_{0.95}M_{0.05}O_2$ (*M* = Sb, Ti, Si, Al, and Mg) along with dopant distributions in $LiNi_{0.95}M_{0.05}O_2$. Each structure has 46,080 atoms. Only Ni and dopant sites are shown, and the size of the dopant is enlarged to show the dopant distribution behavior. A dopant−dopant bond is added when the bond distance is less than 5.5 Å.

structures (each has 46,080 atoms). We find that Sb and Ti tend to aggregate while Si, Al, and Mg distribute randomly in $LiNi_{1-y}M_yO_2$. To quantitatively differentiate the dopant distribution behavior, we calculate the dopant−dopant coordination numbers from the radial distribution functions, see Figure 3. The aggregating dopants, Sb and Ti, exhibit rapidly rising coordination numbers, as a function of dopant−dopant distance, as compared to those of Si, Al, and Mg. It should be noted that the dopant distribution is similar at other doping concentrations (see Figure S5) and in 1,440-atom structures that are used in the grand canonical Monte Carlo (GCMC) simulations.

In Figure 4a−e, we plot the temperature−composition phase diagrams for Sb-, Ti-, Si- Al-, and Mg-doped $Li_{1-x}Ni_{0.95}M_{0.05}O_2$. The phase diagrams clearly show the single-phase regions and two-phase regions in $Li_{1-x}Ni_{0.95}M_{0.05}O_2$ structures. Neither the O1 nor the O1-3 phase appears in the phase diagram of Sb- or Ti-doped $Li_{1-x}Ni_{0.95}M_{0.05}O_2$, but one exists in the phase diagram of Si-, Al-, or Mg-doped $Li_{1-x}Ni_{0.95}M_{0.05}O_2$ after 75% delithiation. For less than 75% delithiation ($x < 0.75$), the single-phase and two-phase regions in Sb-, Ti-, Al-, or Mg-doped $Li_{1-x}Ni_{0.95}M_{0.05}O_2$ are similar to those in pristine $Li_{1-x}NiO_2$ and are all in O3 host structures, without the presence of the O1 phase. On the other hand, $Li_{1-x}Ni_{0.95}Si_{0.05}O_2$ structures exhibit a wide solid solution region for $x < 0.5$. Upon further delithiation ($x > 0.75$), all $Li_{1-x}Ni_{0.95}M_{0.05}O_2$ structures exhibit a two-phase region. Interestingly, the two-phase region in Sb- or Ti-doped $Li_{1-x}Ni_{0.95}M_{0.05}O_2$ is formed between two O3 structures with different Li orderings, which indicates that Sb and Ti can effectively stabilize the O3 host structure during the entire delithiation procedure. On the other hand, in Si-, Al-, or Mg-doped $Li_{1-x}Ni_{0.95}M_{0.05}O_2$, a two-phase region comprising O3+O1-3 or O3+O1 phase appears, which indicates the existence of the O1 oxygen stacking that contributes to the structural vulnerability. In Figure 4f−j, we plot the calculated voltage profiles at 300 and 900 K as a function of discharge capacity and composition for $Li_{1-x}Ni_{0.95}M_{0.05}O_2$. The predicted voltage profiles all exhibit pronounced steps and plateaus which correspond to the intermediate single-phase and two-phase regions in the phase diagrams. In addition, we explore

https://doi.org/10.1021/acsenergylett.3c00169
ACS Energy Lett. 2023, 8, 2401−2407

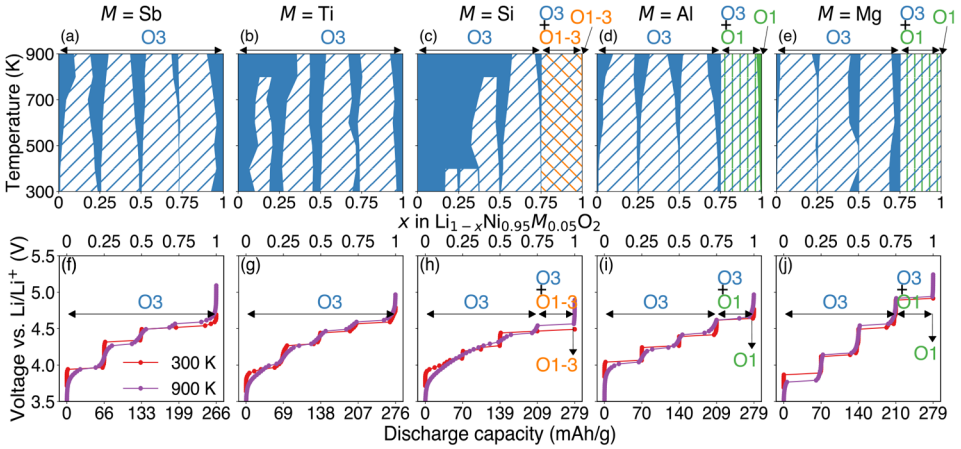

Figure 4. Calculated temperature−composition phase diagrams of (a) Sb-, (b) Ti-, (c) Si-, (d) Al-, and (e) Mg-doped $Li_{1-x}Ni_{0.95}M_{0.05}O_2$ systems. Blue, orange, and green represent O3, O1-3, and O1 phases, respectively. Calculated voltage profiles of (f) Sb-, (g) Ti-, (h) Si-, (i) Al-, and (j) Mg-doped $Li_{1-x}Ni_{0.95}M_{0.05}O_2$. Red and purple curves represent the voltage curves at 300 and 900 K, respectively.

the doping concentration effect on the phase stability of Si-, Al-, and Mg-doped structures by increasing the doping concentration to 10%. In Figure S1, we plot the phase diagrams and voltage profiles of Si-, Al-, and Mg-doped $Li_{1-x}Ni_{0.9}M_{0.1}O_2$. It can be seen that, with a 10% dopant concentration, the O1 phase is prevented in Al- or Mg-doped $Li_{1-x}Ni_{0.9}M_{0.1}O_2$ phase diagram and the O3 host structure is stabilized during the entire delithiation process. On the other hand, the O3+O1-3 two-phase region still persists in $Li_{1-x}Ni_{0.9}Si_{0.1}O_2$ after 75% delithiation. The 10% Al-doping requirement agrees nicely with a previous theoretical study.[28] Experimentally, it has been shown that a 5% Al or Mg dopant concentration decreases the intensity of the O3-to-O1 phase transition in $LiNiO_2$; however, this phase transition virtually disappears with a 10% Al or Mg dopant.[29,30]

In addition, it should be noted that the inclusion of Al^{3+} or Mg^{2+} leads to a direct reduction in available Ni^{3+} redox capability due to charge compensation. During Li deintercalation, Ni^{3+} sites are oxidized to Ni^{4+}, and charging beyond the Ni^{3+} redox capability typically results in oxygen redox, which is associated with oxygen release and structural damages. Therefore, for $Li_{1-x}Ni_{0.9}Al_{0.1}O_2$, the delithiation should be limited to 90% ($x \leq 0.9$, 255 mAh/g) and 80% delithiation ($x \leq 0.8$, 227 mAh/g) for $Li_{1-x}Ni_{0.9}Mg_{0.1}O_2$. A similar recommendation has also been reported in a previous experimental study.[29]

Overall, we predict that Sb and Ti favor dopant aggregation in $LiNi_{1-y}M_yO_2$ bulk structure and stabilize the O3 host structure during the delithiation process. We find that the dopant-enriched aggregates have a beneficial effect in suppressing the formation of the O1 phase, therefore enhancing the structural stability of the cathode. Interestingly, using dopant aggregates to enhance the mechanical strength of the layered cathode and suppress cracking has also been reported in Mg-doped $Na_{0.67}Ni_{0.33}Mn_{0.67}O_2$.[32] On the other hand, Si, Al, and Mg tend to distribute homogeneously throughout the cathode particles. The use of Al or Mg requires a higher doping concentration to effectively prevent the formation of the O1 phase, and Si is ineffective in stabilizing the O3 host structure, even with a higher doping concentration. The benefit of a higher doping concentration has also been experimentally confirmed in Al-doped $LiNiO_2$, where a sufficient amount of Al doping (≥5%) is needed to reduce the detrimental effect of the O3-to-O1 phase transition.[18]

The tendency toward different dopant distributions is reflected in the effective cluster interaction (ECI) values from the fitted cluster-expansion models. In Figure S2, we plot the estimated ECI values of two-site dopant−dopant clusters as a function of pair distance. We observe that both Sb and Ti exhibit negative ECI values, which gradually become less negative with dopant−dopant pair distance and indicate attractive dopant−dopant pair interactions. The Ti−Ti and Sb−Sb ECIs reflect the aggregation behavior of Sb and Ti in $LiNi_{1-y}M_yO_2$ bulk structure. Conversely, Si−Si, Al−Al, and Mg−Mg exhibit positive ECI values, especially when the two dopants occupy nearest-neighbor sites, which indicate repulsive dopant−dopant pair interactions. As a result, the repulsive dopant−dopant interactions favor a uniform dopant distribution in Si-, Al-, or Mg-doped $LiNi_{1-y}M_yO_2$. The details of our cluster-expansion settings of pristine and doped $LiNiO_2$ can be found in Table S1. The tendency toward dopant aggregation is likely attributable to a combination of electrostatic and size effects. For example, the Sb^{5+}−Sb^{5+} pair interaction is expected to be less electrostatically favorable than the Sb^{5+}−Ni^{3+} pair; however, the overall attractive Sb−Sb pair interactions imply that the electrostatic effect does not dominate the dopant aggregation behavior. On the other hand, the dopants exhibit different ionic sizes (see Table S2), which induce different amounts of local strain in the bulk of $LiNiO_2$, especially if the dopants aggregate. Indeed, the ionic radii of Sb^{5+}, Ti^{4+}, and Al^{3+} are similar to that of Ni^{3+}, whereas Si^{4+} is much smaller than Ni^{3+}, and Mg^{2+} is significantly larger than Ni^{3+}.[33] Figure S3 shows that the octahedron formed by Si, Al, or Mg exhibits a larger octahedral volume difference between the dopant and Ni as compared to the Sb or Ti octahedron. As a result, an energy penalty is associated with any aggregate of Si, Al, or Mg,[34] which favors a more random dopant distribution of Si, Al, or Mg. Except for Al^{3+}, a large size difference between the dopant and Ni^{3+} corresponds to a large volume difference of local octahedrons formed by dopant and Ni. More dopants with ionic radii similar to that of Ni^{3+}, such as W^{6+}, Nb^{5+}, Ta^{5+}, and Mo^{6+}, are recommended for exploration. Nonetheless, recent experimental studies also reported a homogeneous dopant distribution in Mg-doped Ni-rich oxides[15,35] and Al-doped Li- and Mn-rich oxides.[21] Both

https://doi.org/10.1021/acsenergylett.3c00169
ACS Energy Lett. 2023, 8, 2401−2407

dopants have been found to improve the cathode bulk stability at a highly delithiated state. Our recent study of Sb-doped $LiNiO_2$ found that Sb tends to aggregate toward the cathode surface with a hierarchical Sb distribution.[3] The surface enrichment of Sb can effectively mitigate the oxygen-loss-induced surface densification and therefore improve the cycling performance. In this study, we further demonstrate that Sb improves the structural stability of $LiNiO_2$ by preventing the onset of the O1 phase at high charge. Such combined surface and bulk stabilization effects from the dopants have also been reported in Ti-,[15,36] Ta-,[37] W-,[13] or Mo-doped[38] Ni-rich cathodes and in Nb-doped[39] Li-rich disordered rocksalt oxide. Interestingly, these dopants all exhibit a hierarchical distribution with an aggregation at the cathode surface.

Combining our current study and the previous reports, we propose materials design principles governing dopant selection for Ni-rich oxide cathodes. High-valence dopants with ionic radii similar to that of Ni^{3+} tend to exhibit a hierarchical distribution with an aggregation at the cathode surface and, therefore, may stabilize both the surface and bulk of Ni-rich oxide cathodes and improve the cycling performance. A recent study by Park et al.[12] reported that doping high-valence ions delays and suppresses the O3-to-O1 phase transition in $LiNi_{0.9}Mn_{0.1}O_2$ cathode, therefore dissipating the deleterious strain-induced microcracks and enhancing the cycling stability. Despite the excellent agreements with the experimental results, it should be noted that the structural models used in this study are simplified compared with those observed in experiments:

(1) We assume no Li−Ni cation mixing in as-synthesized pristine or doped $LiNiO_2$. On the other hand, regardless of the synthesis method, $LiNiO_2$ is usually found to be Li-deficient and Ni^{2+}-excessive, which yields an overall $Li_{1-z}Ni_{1+z}O_2$ composition with the smallest departure from stoichiometry at $z = 0.015-0.02$,[40,41] with an extra z Ni^{2+} in the Li-layer, due to the similar sizes of Li^+ and Ni^{2+}. The degree of Li−Ni cation mixing could be further increased with introducing doping elements, especially high-valence dopants, as the charge balance is achieved by generating more Ni^{2+} ions.[12]

(2) We assume no interlayer or intralayer dopant migration during cycling such that the dopant positions are fixed at the NiO_2 layers during GCMC simulations. However, Mg dopants have been reported in both the Li layer and the transition metal layer.[15,42] Additionally, the presence of dopants in the Li layer may act as pillaring ions at delithiated states at high voltages, reducing the large anisotropic lattice distortion and enhancing structural stability.[42] In Figure S4, we plot the calculated unit cell volumes as a function of Li concentration for pristine $Li_{1-x}NiO_2$ and $Li_{1-x}Ni_{0.95}M_{0.05}O_2$ at 300 K. We observe a large lattice contraction beyond 75% delithiation, associated with NiO_2 appearance, across all the considered cathode chemistries. The lattice contraction is only marginally improved with Sb and Ti doping.

(3) The impact of oxygen evolution on the phase transition at a high charge state is not considered. Recently, Park et al.[43] reported that the O3-to-O1 phase transition in $LiNiO_2$ is more severe in the surface region of the cathode than in the bulk region, due to a higher concentration of oxygen vacancies near the surface. Wang et al.[8−10] also demonstrated that the O1 phase is more vulnerable to oxygen loss as compared to the O3 phase. The oxygen loss lowers the energy barrier of Ni migration into the Li layer, thereby facilitating a transformation from the layered structure into a densified rocksalt structure and compromising reversibility of the O3-to-O1 transition.

In summary, using a first-principles, cluster-expansion and Monte Carlo approach, we have obtained temperature−composition phase diagrams for pristine and Sb-, Ti-, Si- Al-, and Mg-doped $LiNiO_2$. We find, in agreement with experiments, that in pristine $LiNiO_2$ the structural instability appears after 75% delithiation due to the formation of the O1 oxygen stacking in the structure. The O3-to-O1 phase transition is found to be effectively prevented in Sb- or Ti-doped $LiNiO_2$, even with a small dopant concentration, i.e., less than 5%. On the other hand, we find that a higher dopant concentration of Al or Mg is necessary, i.e., at least 10%, to prevent the O3-to-O1 phase transition. We also find that Si doping is ineffective in stabilizing the O3 phase. Interestingly, Sb and Ti tend to aggregate in $LiNiO_2$ due to an attractive dopant−dopant interaction, whereas Si, Al, and Mg exhibit a uniform distribution behavior. Such dopant-enriched aggregates are shown to effectively prevent the O1 phase formation and stabilize the O3 host structure during the delithiation process, which has experimentally been shown to correlate with improved cycling performance. Overall, we attribute the factors modulating the suppression of the O3-to-O1 phase transition to a combination of dopant aggregation and concentration. For the concentrations examined here (2.5% to 10%), a dopant aggregate of Si, Al, or Mg in $LiNiO_2$ is found to be thermodynamically unfavorable, partially due to local strain effects. Dopant aggregates with Sb or Ti are found to beneficially prevent the formation of the O1 phase, while a higher concentration of homogeneously distributed Al or Mg is needed to achieve the same effect. However, while a higher concentration (10%) of Al or Mg can stabilize the O3 phase, we note that a higher dopant concentration also lowers the discharge capacity, as redox-active Ni is replaced with a redox-inactive dopant. Based on these results, we propose to introduce high-valence dopants with ionic radii similar to that of Ni^{3+} into the Ni-rich oxide cathodes to stabilize the cathode bulk structure. These dopants include W^{6+}, Mo^{6+}, V^{5+}, Nb^{5+}, Ta^{5+}, Sb^{5+}, Ti^{4+}, Mn^{4+}, and Ge^{4+}. In addition, the dopants may aggregate at the cathode surface and form a hierarchical distribution that could stabilize both the surface and bulk of the cathode particles. The derived materials design principles not only provide guidance on doping engineering of Ni-rich, Co-free cathodes but also shed light on stabilizing the bulk structure of all high-energy-density cathodes.

■ ASSOCIATED CONTENT

Supporting Information

The Supporting Information is available free of charge at https://pubs.acs.org/doi/10.1021/acsenergylett.3c00169.

Computational details, Shannon effective ionic radii, cluster-expansion settings, calculated voltage profiles and phase diagrams, effective cluster interaction values, octahedral volume difference, calculated unit cell volumes, amd dopant distributions (PDF)

■ AUTHOR INFORMATION

Corresponding Author

Kristin A. Persson − *Department of Materials Science and Engineering, University of California, Berkeley, California 94720-1760, United States; Energy Storage and Distributed Resources Division, Lawrence Berkeley National Laboratory, Berkeley, California 94720, United States; Molecular Foundry, Lawrence Berkeley National Laboratory, Berkeley,*

California 94720, United States; orcid.org/0000-0003-2495-5509; Email: kapersson@lbl.gov

Authors

Jianli Cheng − *Energy Storage and Distributed Resources Division, Lawrence Berkeley National Laboratory, Berkeley, California 94720, United States;* orcid.org/0000-0002-0302-7861

Bin Ouyang − *Department of Chemistry and Biochemistry, Florida State University, Tallahassee, Florida 32306, United States*

Complete contact information is available at: https://pubs.acs.org/10.1021/acsenergylett.3c00169

Notes

The authors declare no competing financial interest.

■ ACKNOWLEDGMENTS

The authors thank Dr. Tina Chen, Peichen Zhong, Fengyu Xie, Dr. Luis Barroso-Luque, Dr. Yoyo Hinuma, Dr. Chunyang Wang and Dr. Huolin Xin for useful discussions. This work was supported by the U.S. Department of Energy's Office of Energy Efficiency and Renewable Energy (EERE) under the Award Number DE-EE0008444. The research was performed using computational resources sponsored by the Department of Energy's Office of Energy Efficiency and Renewable Energy and located at the National Renewable Energy Laboratory.

■ REFERENCES

(1) BloombergNEF, EVO Report 2022, https://about.bnef.com/electric-vehicle-outlook/ (accessed 01/23/2023).

(2) Li, W.; Lee, S.; Manthiram, A. High-Nickel NMA: A Cobalt-Free Alternative to NMC and NCA Cathodes for Lithium-Ion Batteries. *Adv. Mater.* **2020**, *32*, 2002718.

(3) Cheng, J.; Mu, L.; Wang, C.; Yang, Z.; Xin, H. L.; Lin, F.; Persson, K. A. Enhancing surface oxygen retention through theory-guided doping selection in $Li_{1-x}NiO_2$ for next-generation lithium-ion batteries. *J. Mater. Chem. A* **2020**, *8*, 23293−23303.

(4) Yoon, C. S.; Jun, D.-W.; Myung, S.-T.; Sun, Y.-K. Structural Stability of $LiNiO_2$ Cycled above 4.2 V. *ACS Energy Letters* **2017**, *2*, 1150−1155.

(5) Cheng, J.; Fong, K. D.; Persson, K. A. Materials design principles of amorphous cathode coatings for lithium-ion battery applications. *J. Mater. Chem. A* **2022**, *10*, 22245−22256.

(6) Ohzuku, T.; Ueda, A.; Nagayama, M. Electrochemistry and Structural Chemistry of $LiNiO_2$ (R3m) for 4 V Secondary Lithium Cells. *J. Electrochem. Soc.* **1993**, *140*, 1862−1870.

(7) Li, H.; Zhang, N.; Li, J.; Dahn, J. R. Updating the Structure and Electrochemistry of Li_xNiO_2 for $0 \leq x \leq 1$. *J. Electrochem. Soc.* **2018**, *165*, A2985−A2993.

(8) Wang, C.; Zhang, R.; Kisslinger, K.; Xin, H. L. Atomic-Scale Observation of O1 Faulted Phase-Induced Deactivation of $LiNiO_2$ at High Voltage. *Nano Lett.* **2021**, *21*, 3657−3663.

(9) Wang, C.; Wang, X.; Zhang, R.; Lei, T.; Kisslinger, K.; Xin, H. L. Resolving complex intralayer transition motifs in high-Ni-content layered cathode materials for lithium-ion batteries. *Nat. Mater.* **2023**, *22*, 235−241.

(10) Wang, C.; Wang, X.; Zou, P.; Zhang, R.; Wang, S.; Song, B.; Low, K.-B.; Xin, H. L. Direct observation of chemomechanical stress-induced phase transformation in high-Ni layered cathodes for lithium-ion batteries. *Matter* **2023**, *6*, 1265−1277.

(11) Zhang, R.; Wang, C.; Zou, P.; Lin, R.; Ma, L.; Yin, L.; Li, T.; Xu, W.; Jia, H.; Li, Q.; Sainio, S.; Kisslinger, K.; Trask, S. E.; Ehrlich, S. N.; Yang, Y.; Kiss, A. M.; Ge, M.; Polzin, B. J.; Lee, S. J.; Xu, W.; Ren, Y.; Xin, H. L. Compositionally complex doping for zero-strain zero-cobalt layered cathodes. *Nature* **2022**, *610*, 67−73.

(12) Park, G. T.; Namkoong, B.; Kim, S. B.; Liu, J.; Yoon, C. S.; Sun, Y. K. Introducing high-valence elements into cobalt-free layered cathodes for practical lithium-ion batteries. *Nat. Energy* **2022**, *7*, 946−954.

(13) Ryu, H.-H.; Park, G.-T.; Yoon, C. S.; Sun, Y.-K. Suppressing Detrimental Phase Transitions via Tungsten Doping of $LiNiO_2$ Cathode for Next-generation Lithium-ion Batteries. *J. Mater. Chem. A* **2019**, *7*, 18580−18588.

(14) Huang, G.-X.; Wang, R.-H.; Lv, X.-Y.; Su, J.; Long, Y.-F.; Qin, Z.-Z.; Wen, Y.-X. Effect of Niobium Doping on Structural Stability and Electrochemical Properties of $LiNiO_2$ Cathode for Li-Ion Batteries. *J. Electrochem. Soc.* **2022**, *169*, 040533.

(15) Mu, L.; Zhang, R.; Kan, W. H.; Zhang, Y.; Li, L.; Kuai, C.; Zydlewski, B.; Rahman, M. M.; Sun, C. J.; Sainio, S.; Avdeev, M.; Nordlund, D.; Xin, H. L.; Lin, F. Dopant Distribution in Co-Free High-Energy Layered Cathode Materials. *Chem. Mater.* **2019**, *31*, 9769−9776.

(16) Xu, T.; Du, F.; Wu, L.; Fan, Z.; Shen, L.; Zheng, J. Boosting the electrochemical performance of $LiNiO_2$ by extra low content of Mn-doping and its mechanism. *Electrochim. Acta* **2022**, *417*, 140345.

(17) Kitsche, D.; Schweidler, S.; Mazilkin, A.; Geßwein, H.; Fauth, F.; Suard, E.; Hartmann, P.; Brezesinski, T.; Janek, J.; Bianchini, M. The effect of gallium substitution on the structure and electrochemical performance of $LiNiO_2$ in lithium-ion batteries. *Mater. Adv.* **2020**, *1*, 639−647.

(18) Cao, H.; Du, F.; Adkins, J.; Zhou, Q.; Dai, H.; Sun, P.; Hu, D.; Zheng, J. Al-doping induced superior lithium ion storage capability of $LiNiO_2$ spheres. *Ceram. Int.* **2020**, *46*, 20050−20060.

(19) Kong, X.-Z.; Li, D.-L.; Lahtinen, K.; Kallio, T.; Ren, X.-Q. Effect of Copper-Doping on $LiNiO_2$ Positive Electrode for Lithium-Ion Batteries. *J. Electrochem. Soc.* **2020**, *167*, 140545.

(20) Levartovsky, Y.; Kunnikuruvan, S.; Chakraborty, A.; Maiti, S.; Grinblat, J.; Talianker, M.; Major, D. T.; Aurbach, D. Electrochemical and Structural Studies of $LiNi_{0.85}Co_{0.1}Mn_{0.05}O_2$, a Cathode Material for High Energy Density Li-Ion Batteries, Stabilized by Doping with Small Amounts of Tungsten. *J. Electrochem. Soc.* **2021**, *168*, 060552.

(21) Nayak, P. K.; Grinblat, J.; Levi, M.; Levi, E.; Kim, S.; Choi, J. W.; Aurbach, D. Al Doping for Mitigating the Capacity Fading and Voltage Decay of Layered Li and Mn-Rich Cathodes for Li-Ion Batteries. *Adv. Energy Mater.* **2016**, *6*, 1502398.

(22) Guilmard, M.; Rougier, A.; Grüne, M.; Croguennec, L.; Delmas, C. Effects of aluminum on the structural and electrochemical properties of $LiNiO_2$. *J. Power Sources* **2003**, *115*, 305−314.

(23) Kim, U. H.; Jun, D. W.; Park, K. J.; Zhang, Q.; Kaghazchi, P.; Aurbach, D.; Major, D. T.; Goobes, G.; Dixit, M.; Leifer, N.; Wang, C. M.; Yan, P.; Ahn, D.; Kim, K. H.; Yoon, C. S.; Sun, Y. K. Pushing the limit of layered transition metal oxide cathodes for high-energy density rechargeable Li ion batteries. *Energy Environ. Sci.* **2018**, *11*, 1271−1279.

(24) Yoon, C. S.; Choi, M.-J.; Jun, D.-W.; Zhang, Q.; Kaghazchi, P.; Kim, K.-H.; Sun, Y.-K. Cation Ordering of Zr-Doped $LiNiO_2$ Cathode for Lithium-Ion Batteries. *Chem. Mater.* **2018**, *30*, 1808−1814.

(25) Kong, D.; Hu, J.; Chen, Z.; Song, K.; Li, C.; Weng, M.; Li, M.; Wang, R.; Liu, T.; Liu, J.; Zhang, M.; Xiao, Y.; Pan, F. Ti-Gradient Doping to Stabilize Layered Surface Structure for High Performance High-Ni Oxide Cathode of Li-Ion Battery. *Adv. Energy Mater.* **2019**, *9*, 1901756.

(26) Yoshida, T.; Hongo, K.; Maezono, R. First-Principles Study of Structural Transitions in $LiNiO_2$ and High-Throughput Screening for Long Life Battery. *J. Phys. Chem. C* **2019**, *123*, 14126−14131.

(27) Kong, F.; Liang, C.; Longo, R. C.; Yeon, D.-H.; Zheng, Y.; Park, J.-H.; Doo, S.-G.; Cho, K. Conflicting Roles of Anion Doping on the Electrochemical Performance of Li-Ion Battery Cathode Materials. *Chem. Mater.* **2016**, *28*, 6942−6952.

(28) Mock, M.; Bianchini, M.; Fauth, F.; Albe, K.; Sicolo, S. Atomistic understanding of the $LiNiO_2$−NiO_2 phase diagram from experimentally guided lattice models. *J. Mater. Chem. A* **2021**, *9*, 14928−14940.

(29) Faenza, N. V.; Pereira, N.; Halat, D. M.; Vinckeviciute, J.; Bruce, L.; Radin, M. D.; Mukherjee, P.; Badway, F.; Halajko, A.; Cosandey, F.; Grey, C. P.; Van Der Ven, A.; Amatucci, G. G. Phase Evolution and Degradation Modes of R3 m $Li_xNi_{1-y-z}Co_yAl_zO_2$ Electrodes Cycled Near Complete Delithiation. *Chem. Mater.* **2018**, *30*, 7545−7574.
(30) Li, H.; Cormier, M.; Zhang, N.; Inglis, J.; Li, J.; Dahn, J. R. Is Cobalt Needed in Ni-Rich Positive Electrode Materials for Lithium Ion Batteries? *J. Electrochem. Soc.* **2019**, *166*, A429−A439.
(31) Arroyo y de Dompablo, M. E.; Van der Ven, A.; Ceder, G. First-principles calculations of lithium ordering and phase stability on Li_xNiO_2. *Phys. Rev. B* **2002**, *66*, 064112.
(32) Wang, K.; Wan, H.; Yan, P.; Chen, X.; Fu, J.; Liu, Z.; Deng, H.; Gao, F.; Sui, M. Dopant Segregation Boosting High-Voltage Cyclability of Layered Cathode for Sodium Ion Batteries. *Adv. Mater.* **2019**, *31*, 1904816.
(33) Shannon, R. Revised effective ionic radii and systematic studies of interatomic distances in halides and chalcogenides. *Acta Crystallogr., Sect. A* **1976**, *32*, 751−767.
(34) Croguennec, L.; Shao-Horn, Y.; Gloter, A.; Colliex, C.; Guilmard, M.; Fauth, F.; Delmas, C. Segregation Tendency in Layered Aluminum-Substituted Lithium Nickel Oxides. *Chem. Mater.* **2009**, *21*, 1051−1059.
(35) Li, H.; Zhou, P.; Liu, F.; Li, H.; Cheng, F.; Chen, J. Stabilizing nickel-rich layered oxide cathodes by magnesium doping for rechargeable lithium-ion batteries. *Chemical Science* **2019**, *10*, 1374−1379.
(36) Steiner, J. D.; Cheng, H.; Walsh, J.; Zhang, Y.; Zydlewski, B.; Mu, L.; Xu, Z.; Rahman, M. M.; Sun, H.; Michel, F. M.; Sun, C.-J.; Nordlund, D.; Luo, W.; Zheng, J.-C.; Xin, H. L.; Lin, F. Targeted Surface Doping with Reversible Local Environment Improves Oxygen Stability at the Electrochemical Interfaces of Nickel-Rich Cathode Materials. *ACS Appl. Mater. Interfaces* **2019**, *11*, 37885−37891.
(37) Jamil, S.; Yu, R.; Wang, Q.; Fasehullah, M.; Huang, Y.; Yang, Z.; Yang, X.; Wang, X. Enhanced cycling stability of nickel-rich layered oxide by tantalum doping. *J. Power Sources* **2020**, *473*, 228597.
(38) Breuer, O.; Chakraborty, A.; Liu, J.; Kravchuk, T.; Burstein, L.; Grinblat, J.; Kauffman, Y.; Gladkih, A.; Nayak, P.; Tsubery, M.; Frenkel, A. I.; Talianker, M.; Major, D. T.; Markovsky, B.; Aurbach, D. Understanding the Role of Minor Molybdenum Doping in $LiNi_{0.5}Co_{0.2}Mn_{0.3}O_2$ Electrodes: From Structural and Surface Analyses and Theoretical Modeling to Practical Electrochemical Cells. *ACS Appl. Mater. Interfaces* **2018**, *10*, 29608−29621.
(39) Cambaz, M. A.; Vinayan, B. P.; Geßwein, H.; Schiele, A.; Sarapulova, A.; Diemant, T.; Mazilkin, A.; Brezesinski, T.; Behm, R. J.; Ehrenberg, H.; Fichtner, M. Oxygen Activity in Li-Rich Disordered Rock-Salt Oxide and the Influence of $LiNbO_3$ Surface Modification on the Electrochemical Performance. *Chem. Mater.* **2019**, *31*, 4330−4340.
(40) Delmas, C.; Pérès, J. P.; Rougier, A.; Demourgues, A.; Weill, F.; Chadwick, A.; Broussely, M.; Perton, F.; Biensan, P.; Willmann, P. On the behavior of the Li_xNiO_2 system: an electrochemical and structural overview. *J. Power Sources* **1997**, *68*, 120−125.
(41) Rougier, A.; Gravereau, P.; Delmas, C. Optimization of the Composition of the $Li_{1-z}Ni_{1+z}O_2$ Electrode Materials: Structural, Magnetic, and Electrochemical Studies. *J. Electrochem. Soc.* **1996**, *143*, 1168−1175.
(42) Xie, Q.; Li, W.; Manthiram, A. A Mg-Doped High-Nickel Layered Oxide Cathode Enabling Safer, High-Energy-Density Li-Ion Batteries. *Chem. Mater.* **2019**, *31*, 938−946.
(43) Park, K. Y.; Zhu, Y.; Torres-Castanedo, C. G.; Jung, H. J.; Luu, N. S.; Kahvecioglu, O.; Yoo, Y.; Seo, J. W. T.; Downing, J. R.; Lim, H. D.; Bedzyk, M. J.; Wolverton, C.; Hersam, M. C. Elucidating and Mitigating High-Voltage Degradation Cascades in Cobalt-Free $LiNiO_2$ Lithium-Ion Battery Cathodes. *Adv. Mater.* **2022**, *34*, 2106402.

https://doi.org/10.1021/acsenergylett.3c00169
ACS Energy Lett. 2023, 8, 2401−2407